Biomicrofluidics ARTICLE scitation.org/journal/bmf

Resolving dynamics of inertial migration in straight and curved microchannels by direct cross-sectional imaging

Cite as: Biomicrofluidics **15**, 014101 (2021); doi: 10.1063/5.0032653
Submitted: 9 October 2020 · Accepted: 9 December 2020 ·
Published Online: 4 January 2021

Jian Zhou and Ian Papautsky[a)]

AFFILIATIONS

Department of Bioengineering, University of Illinois at Chicago, 851 S. Morgan Street, 218 SEO, Chicago, Illinois 60607, USA

[a)]**Author to whom correspondence should be addressed:** papauts@uic.edu. **Tel.:** +1 312 413 3800

ABSTRACT

The explosive development of inertial microfluidic systems for label-free sorting and isolation of cells demands improved understanding of the underlying physics that dictate the intriguing phenomenon of size-dependent migration in microchannels. Despite recent advances in the physics underlying inertial migration, migration dynamics in 3D is not fully understood. These investigations are hampered by the lack of easy access to the channel cross section. In this work, we report on a simple method of direct imaging of the channel cross section that is orthogonal to the flow direction using a common inverted microscope, providing vital information on the 3D cross-sectional migration dynamics. We use this approach to revisit particle migration in both straight and curved microchannels. In the rectangular channel, the high-resolution cross-sectional images unambiguously confirm the two-stage migration model proposed earlier. In the curved channel, we found two vertical equilibrium positions and elucidate the size-dependent vertical and horizontal migration dynamics. Based on these results, we propose a critical ratio of blockage ratio (β) to Dean number (De) where no net lateral migration occurs ($\beta/De \sim 0.01$). This dimensionless number (β/De) predicts the direction of lateral migration (inward or outward) in curved and spiral channels, and thus serves as a guideline in design of such channels for particle and cell separation applications. Ultimately, the new approach to direct imaging of the channel cross section enables a wealth of previously unavailable information on the dynamics of inertial migration, which serves to improve our understanding of the underlying physics.

INTRODUCTION

The intriguing phenomenon of size-dependent migration in inertial microfluidics has been applied to an increasing number of biomedical applications.[1,2] Its propensity for high-throughput processing of biological samples has attracted burgeoning interest in developing and improving inertial microfluidic devices for size-based sorting of particles,[1,2] blood cells,[3,4] circulating tumor cells (CTCs),[5–8] microalgae,[9,10] bacteria,[11,12] and even intracellular organelles such as mitochondria.[13] The label-free precision manipulation capabilities have led to the emergence of microfluidic devices for automated sample preparation, such as solution exchange,[14,15] cell concentration,[16,17] and intracellular delivery.[18] Coupling of the inertial effect and fluid shear has also been used for the characterization of cell biophysical properties.[19] The growing interest in inertial microfluidics demands a full understanding of the underlying mechanisms. Despite recent advances in the physics underlying inertial migration,[20,21] 3D migration dynamics is not fully understood.

A major hurdle that leads to difficulties in achieving a full understanding of inertial migration in 3D is the lack of easy access to channel cross section. Particle streak velocimetry (PSV) is the most common approach to investigating particle migration in microfluidic channels, which readily provides lateral positions and downstream trajectories of focused fluorescent particles. Particle vertical position in cross section, however, is not directly accessible using PSV, although the cross-sectional locations of focused streams can be inferred from top view and side view images using a pair of microchannels [Fig. 1(a)(i)].[22,23] High-speed imaging can also be used to qualitatively estimate the relative vertical positions of particles in bright-field (BF) images.[24,25] Although confocal microscopy is the most accessible way to obtain particle positions in channel cross sections,[26–29] precise particle position cannot be

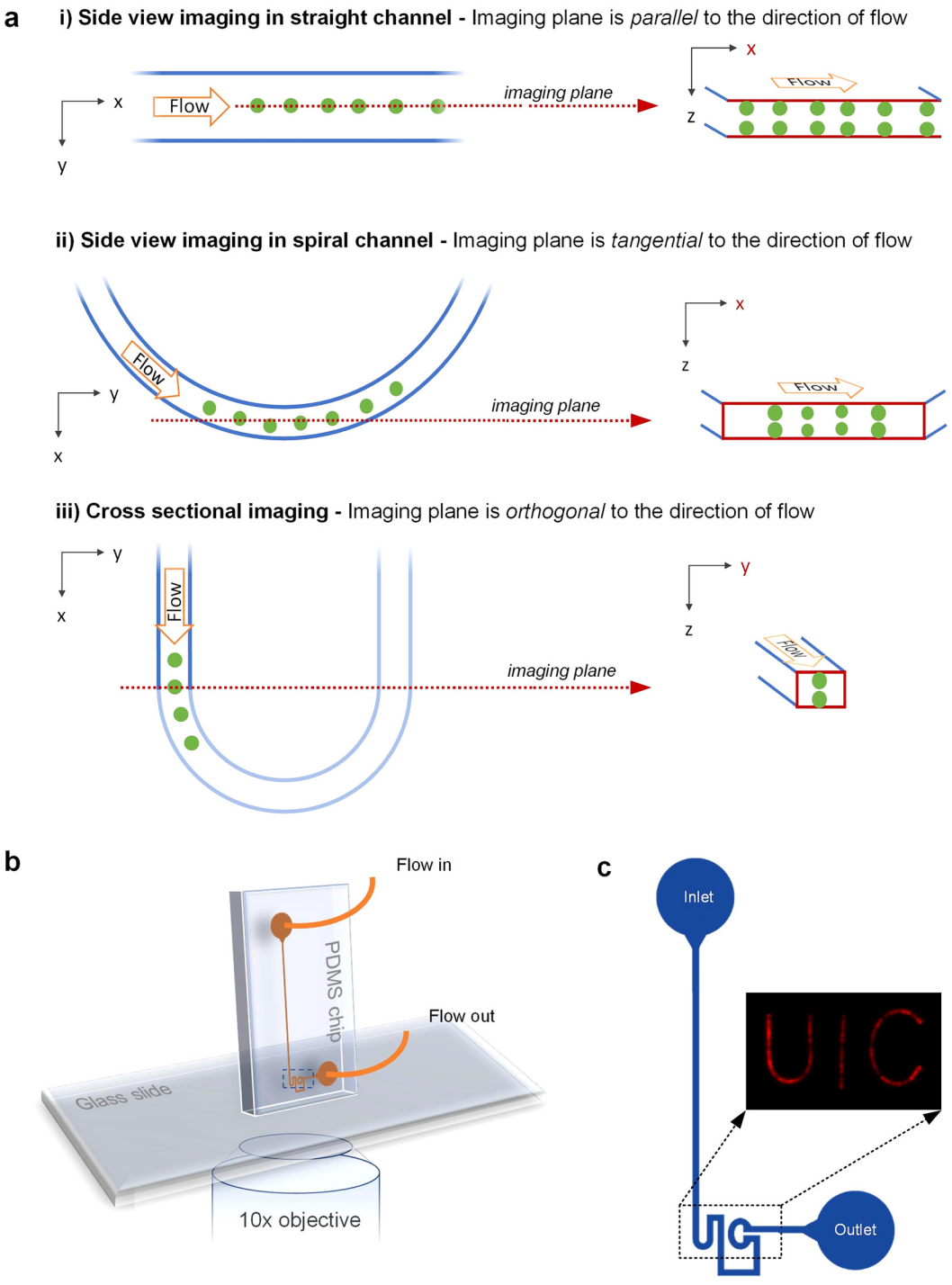

FIG. 1. Imaging microchannel cross section. (a) Schematic illustrations of channel imaging. Our previous work used top view and side view images in straight channels to infer particle focusing positions in the channel cross section (i). Others have used the top view and side view images to infer focusing positions in spiral channels (ii). In this work, we use direct imaging of the channel cross section to resolve the cross-sectional positions of individual particles (iii). In all cases, flow is in the x-direction. (b) Illustration of the PDMS device placement for cross-sectional imaging in this work. The PDMS device was vertically bonded to a glass slide, which was then placed onto the stage of an inverted microscope. (c) Layout of the microchannel used in this work for investigating 3D particle migration dynamics.

determined as the approach is generally not sufficiently fast to capture the entire particle, resulting in distorted clusters of possible focusing positions in reconstructed images of channel cross section. Alternatively, digital holographic microscopy (DHM) can offer access to 3D positions of particles inside a channel, but its large uncertainty in vertical measurements (an order higher than that in horizontal measurements) results in significant measurement error ($\sim 0.2a$, where a is particle diameter),[30,31] limiting the application of DHM to cases of a large blockage ratio ($\beta = a/D_h$, where D_h is the hydraulic diameter of a microchannel). Recently, Nguyen *et al.*[32] reported an approach for imaging particle alignment in a $1.5 \times 1.5 \times 1\text{mm}^2$ chamber from all three directions using a prism. However, their method was applied to static particles only with no flow in the chamber, while the resolution of the approach was not sufficient to resolve the positions of individual particles. Thus far, images of fast-moving particles in microchannel cross sections are not reported in the literature for inertial microfluidics.

In this work, we demonstrate an approach that allows easy observation of channel cross section using a common inverted microscope with a high-speed camera for the investigation of inertial migration dynamics in cross sections of straight and curved microchannels. As shown in Figs. 1(b) and 1(c), a microchannel is placed vertically on the microscope stage with channel cross section directly facing the microscope objective under the stage. A similar concept was reported by Shichi *et al.*[33] for imaging particle focusing in a sub-millimeter square tube using a complex customized setup, and Guan *et al.*[23] for imaging side view of a spiral channel [xz plane in Fig. 1(a)(ii)]. Nevertheless, direct observation of focusing in the cross section that is orthogonal to the flow direction was not achieved in either work.

Herein, we acquire high-resolution bright-field and fluorescent images of particles in a small cross section ($100 \times 50\,\mu\text{m}^2$), which provide precise vertical and lateral positions of particles [Fig. 1(a)(iii)]. The novelty of this method stems for the fact that we directly image the channel cross section (yz plane) orthogonal to the flow direction (x-direction). This is in contrast to the methods used in our early work[22] and by others[23] to image channel side (xz plane), which is parallel to the flow direction. Additionally, we can capture precise particle cross-sectional positions (y, z) directly, while only the particle focusing positions can be inferred from the top view and side view images in previous work.[22,23] Finally, we are able to locate the individual particle positions in the entire channel cross-section, which is not possible using the previously reported indirect methods.[22,23]

Using this approach, we revisited particle migration dynamics in straight and curved rectangular microchannels. First, our cross-sectional view images unambiguously confirm the two-stage migration model that we previously proposed based on PSV in channels with reciprocal ARs.[22] Second, the cross-section images of a U-shaped low AR microchannel ($AR < 1$) reveal a more comprehensive picture of particle migration dynamics. Our new findings reveal (1) two vertical positions which are dynamically moving vertically and laterally in a curved channel, (2) size-dependent vertical positions with smaller particles closer to channel center plane, (3) outward migration with smaller particles closer to the outer sidewall of the channel, (4) non-negligible centrifugal force due to particle-fluid density mismatch, and (5) a critical dimensionless number ($\beta/De \sim 0.01$) for determining particle lateral migration direction, which is applicable to a wide range of channel geometries including spiral channels. We show that the dimensionless number can be a practical guideline in designing spiral channels for separation. In short, the new approach to direct imaging of channel cross section enables a wealth of information previously not available regarding the full migration dynamics in inertial microfluidics, which improves our understanding of the underlying physics and offers additional guidance for the design of separation systems.

EXPERIMENT METHODS

Device fabrication

Microfluidic channels were fabricated in polydimethylsiloxane (PDMS, Sylgard 184, Dow Corning) using the standard soft photolithography process with a dry photoresist. Briefly, we laminated with a 50-μm-thick ADEX film (DJ Microlaminates Inc., USA) on a 3 in. silicon wafer following the procedure in our recent publication.[34] The dry film resist was photolithographically patterned to form channel master, and PDMS was cast on the wafer and cured for 6 h on a 65 °C hotplate. Replicated PDMS channels were then bonded to a plain PDMS slab using surface plasma treatment (PE-50, Plasma Etch Inc.) for 20 s after inlet and outlet holes were manually punched. The edges of the PDMS device were cut flat using a sharp blade and the cutting surface was resurfaced using uncured PDMS to improve optical transparency (Fig. S1 in the supplementary material). Microchannel cross section was $100 \times 50\,\mu\text{m}^2$ ($w \times h$). The inner radius of the U-shaped segment was 65 μm, while the outer radius was 165 μm, putting the channel centerline at 115 μm radius of curvature. The length of the first straight segment upstream to the U-shaped segment was 8 mm. The device geometry was carefully selected such that both straight and curved channels could be examined simultaneously and the upstream straight channel can assist in the investigation of particle migration in the curved channel by pre-focusing particles.

Dimensionless numbers

In this work, we used Reynolds number, Dean number, and blockage ratio for characterization of particle migration dynamics. Reynolds number (Re) measures the relative importance of inertial force and viscous force and is defined as $Re = \rho U_f D_h/\mu$, where ρ and μ are the density and dynamic viscosity of the suspending fluid, D_h is the hydraulic diameter of the channel defined as $D_h = 2wh/(w+h)$, and U_f is the average fluid velocity inside the channel ($U_f = Q/wh$, where Q is the volumetric flow rate). Dean number (De) is defined as $De = Re\sqrt{D_h/(2R)}$, where R is the radius of the curvature ($R = 115\,\mu$m for the U-shaped channel). Since Re scales with flow rate, De can also be expressed in terms of the flow rate Q as follows:

$$De = Q \cdot \left(\frac{\rho}{\mu} \cdot \frac{2}{(w+h)} \sqrt{\frac{D_h}{2R}} \right). \tag{1}$$

Therefore, the scaling factor is determined by the fluid properties and channel geometries. The blockage ratio (β) is the ratio of particle size to the hydraulic diameter of the channel ($\beta = a/D_h$).

Sample preparation

Solutions of polystyrene fluorescent microparticles of different diameters were prepared for this work. A saline buffer was first prepared by mixing 0.6 g of NaCl (Fisher Scientific Inc., USA) with 10 ml of DI water to match the particle's density of 1.06 g/cm^3. The 18.7-μm- and 26.3-μm-diameter particles (Polyscienes Inc, USA) were mixed either with the prepared saline solution or DI water for the final volume fractions of 0.025% and 0.027%, respectively. The 32.3-μm-diameter particles (Spherotech Inc.) were mixed with the saline solution for the final volume fraction of 0.02%. Tween 80 was added at 0.1% v/v (Fisher Scientific, USA) into each final suspension of 10 ml to prevent particle aggregates and channel clogging.

Experimental setup

Two schemes of setup were used to acquire top view and cross-sectional view images of particle migration inside our channel. In the first approach, the fabricated device was laid flat on a glass slide with the channel bottom facing the objective for top view imaging. This is the common scheme reported in the literature, where the inlet and the outlet are on the same plane. In the second approach, the PDMS channel was bonded and placed vertically against the supporting 1-mm-thick glass slide (Fig. 1), letting the channel cross section face the objective for cross-sectional view of particle migration. In this case, the inlet was at the top, while the outlet was at the bottom. The hydrostatic pressure inside the vertical channel is negligible (at least 100× smaller than the pressure drop along the channel). Channel cross section was apparent due to the four sharp corners in BF images and the cross-section boundary in FL images was translated from BF images. For both schemes, sample suspension was injected into the PDMS device using a syringe pump (Legato 200, KD Scientific Inc.) to sustain a stable flow rate. The loaded syringe was connected using 1/16 in. Tygon® tubing (IDEX Health & Science LLC) using proper fittings (IDEX Health & Science LLC) and then secured to the device inlet. The outlet was connected to a tubing into a waste container. A wide range of flow rates (50–1000 μl/min) were used in this work.

Imaging and analysis

Both bright-field (BF) and fluorescent images of particles were recorded for analysis using 10× objective with a 10 mm working distance. The numerical aperture is NA = 0.3. BF images of cross-sectional view were acquired at frame rates ranging from 150 000 fps to 300 000 fps using a high-speed camera (Photron Mini AX200, Photron USA Inc). Fluorescent (FL) images were taken at a frame rate of 125 fps. The 100 μs and 1 μs exposure times were set for acquiring fluorescent and BF images of cross-sectional view, respectively. Exposure time was 10–1000 μs for FL images of the top view. ImageJ® (NIH, USA) was used to obtain stacked images of particle migration trajectories in top view images and of particle focusing dynamics in cross-sectional view images, and to measure particle lateral positions from the top view images and vertical inter-particle distance in the cross section.

RESULTS

Two-stage migration in channel cross section

Channel cross sections can be accurately identified in bright-field images using sharp corners that are readily apparent. Due to the excellent transparency of PDMS, identification of channel walls is not easy in all-PDMS channels. We found that the four corners of a vertically oriented PDMS channel were strikingly sharp in the acquired images. As shown in Fig. 2, we focused the microscope objective on six planes of the vertically placed channel, and in each plane, the cross sections of straight channel segments are easily identified by their four corners. Identification of the cross sections of the curved channel segments (planes 2 and 3 in Fig. 2) is not as straightforward due to reflection and refraction of light at the channel-PDMS interface, but is still possible due to increased contrast presented by the curvature. Note that the dark shadows in the images of planes 2–5 are mainly due to the slight inclination of the channel (channel was not placed ideally vertical) and the partial reflection of light on the surfaces of curved channel segments. Furthermore, the cross-sectional dimensions measured from these images are very accurate. The width and height of the cross section were $99 \pm 1.2\,\mu$m and $52 \pm 1.6\,\mu$m ($n = 8$), respectively. These closely matched the direct measurements from cutting the PDMS channel, which were $101 \pm 1.9\,\mu$m and $51 \pm 0.51\,\mu$m ($n = 12$), respectively. Such an accurate delimitation enabled us to locate particle focusing positions directly within the channel cross section rather than by inference based on the top view and side view images as has been the practice so far.[22,35]

Individual particles were observed near the long channel faces by direct imaging of the cross section. At $Re = 50$, we captured 18.7-μm-diameter particles ($\beta = 0.28$) crossing the imaging plane where four cross sections were present [Fig. 3(a)]. Particles were focused in two symmetrical positions, as shown in cross sections P2, P3, and P4. Particles were buried in the dark background of cross section P1 and thus were not distinguishable in the bright-field image. However, in the fluorescent field, the focused particles were observed in all four cross sections. Note that both bright-field and fluorescent particle images were faint in cross section P3, which is in the middle of a straight channel segment, and the fluorescent image had to be properly thresholded for better visualization. These results directly confirmed the two focusing positions in a rectangular microchannel that we previously inferred from the top view and side view images.[22]

Our further experiments corroborate the two-stage model of particle migration dynamics we proposed earlier.[22] Since imaging of the channel inlet was not possible, limited by objective working distance, we kept our objective focused at the same vertical plane (plane 3 in Fig. 2) and varied flow rate to induce different focusing patterns in the cross section. At low flow rate ($Re = 5$), some particle aggregation in the cross section was observed but focusing of particles could not be discerned [Fig. 3(b)(i)]. Such observation was expected since inertial force is generally weak at low Reynolds number. Particle Reynolds number $Re_p = Re\,(a/Dh)^2 > 1$, is generally required to observe inertial migration,[1] which means that for this channel $Re > 7.1$ is necessary. When the flow rate was doubled ($Re = 11$), we observed particles focused into two layers near the long faces of the cross section [Fig. 3(b)(ii)], which is in agreement with the focusing pattern at the end of Stage I migration.[22]

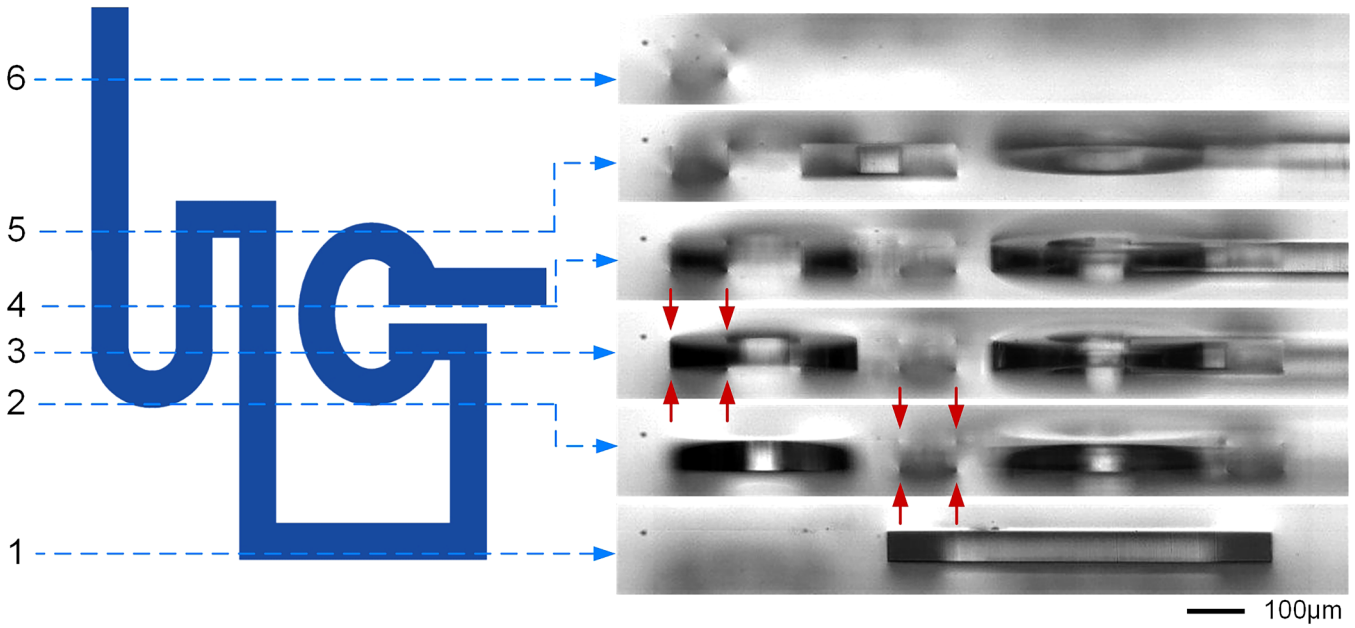

FIG. 2. Six vertical imaging planes in the microchannel and the corresponding bright-field cross-sectional images. Cross sections of the individual microchannels are identified by their four sharp corners (e.g., those indicated by the red arrows). One sharp shallow cross section and two small cross sections are obvious in vertical planes 1 and 2. Multiple cross sections are present in vertical planes 3–5, and only a single cross section is seen in plane 6. The size of the channel cross section was measured to be $52 \times 99\,\mu m^2$ ($n = 8$).

The particle layers did not span the entire channel width, as expected. This suggested that Stage I focusing was already completed and particles were undergoing the Stage II migration. Calculating focusing length for this channel at $Re = 11$ confirms this. Specifically, the channel length before the imaging plane (8 mm) exceeds the focusing length of Stage I (~3 mm), but is less than the full focusing length (~16 mm).[22] Fully focused particles were observed in two positions slightly off-center at $Re = 50$ [Fig. 3(b)(iii)]. This offset is due to the adjacent curved channel which induces inward-only flow in the cross section (see P1 in Fig. S2 in the supplementary material). Therefore, the characteristics of the two-stage migration model have been confirmed by direct imaging of channel cross section. Such collective migration dynamics can be further explained by resolving individual migration pathways, as we describe in our recent work.[45]

3D migration dynamics in curved channels

Inertial migration in curved microchannels, such as spiral and serpentine channels, has been widely used for particle focusing and cell separation since the first demonstrations more than a decade ago.[36–38] In these channels, particles are found to form a single focused stream and its lateral position is highly size-dependent, with larger particles closer to the inner wall of a curved/spiral channel.[37,38] Despite the prominent single stream focusing, the exact focusing positions remain unclear due to the difficulty in observing particles through channel cross section. Early work[25,37] suggested there was a single focusing position in a spiral channel. But later, two major focusing positions were inferred from the stream breakdown at the outlet and from the appearance of particles in images of high-speed camera by Martel and Toner.[24,39] What is more, particle focusing near the outer wall[24,40] was also observed amid the well-accepted thinking that particles should be focused near the inner wall of a spiral channel. All these controversies are mainly due to the lack of access to channel cross section and thus the lack of access to 3D positions of particles.

With the direct access to channel cross section, we can resolve the 3D migration dynamics of particles in curved channels. The commonly used top view fluorescent images show lateral displacement and downstream travel of particles and images of channel cross section provide information on the third dimension, which is vertical movement. For example, top view images in Figs. 4(a) and 4(b) show the 26.3-μm-diameter particles (large $\beta = 0.39$ to ensure full focusing of particles in the upstream straight channel) reach single stream focusing, while the cross-section images [Fig. 4(c)] reveal two vertically symmetrical positions. Although such information can be inferred from fluorescent images of top and side views,[22,23] the cross-section images concurrently provide lateral and vertical positions of particles, which unambiguously shows not only the focusing positions but also the dynamics with changes in flow rate.

As the flow rate increases, particles migrate toward the channel outer wall. We investigated particle migration in the U-shaped channel, with the convenience of constant curvature and the same initial particle positions in the beginning cross section [P1 in Fig. 4(b)] due to the pre-focusing in the upstream straight

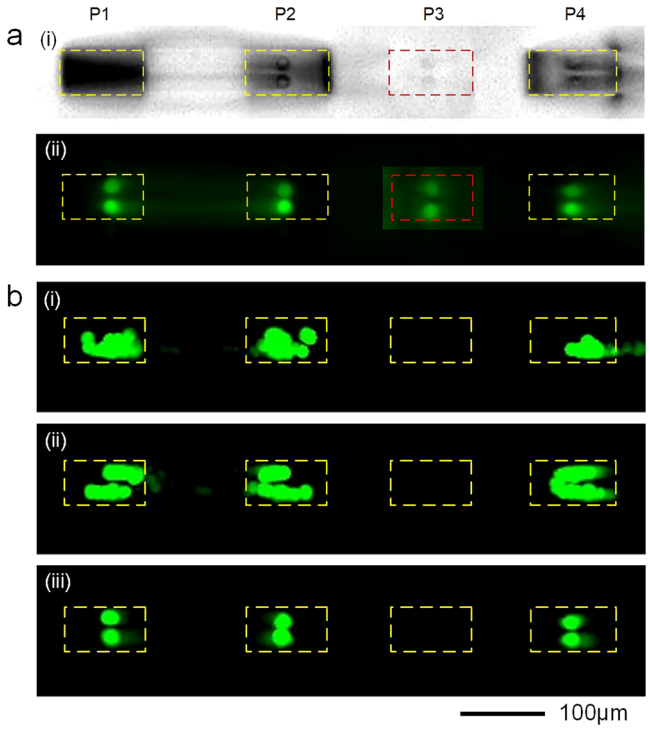

FIG. 3. Particle focusing dynamics captured in the channel cross sections at imaging plane 3. (a) Bright-field and fluorescent images illustrating particles focused in two positions near the top and bottom walls. Note particle images were faint in both fields for the cross section P3 (boundary marked with red dashed line) and the fluorescent intensity was adjusted to show the focusing positions inside the red cross section. Flow rate was 225 μl/min and $Re = 50$. (b) Confirmation of the two-stage migration and focusing of particles in a low aspect ratio rectangular microchannel. (i) Particles initially unfocused at low flow rate ($Re = 5.5$) focus into two lines (ii) upon accomplishing Stage I migration at higher flow rate ($Re = 11$), and further focus into two distinct positions near long walls, and (iii) indicating completion of stage II migration ($Re = 50$). All images were obtained from the same vertical channel position and are stacked from multiple frames of high-speed imaging to show all potential focusing positions. The 18.7-μm-diameter particles were pseudo-colored green.

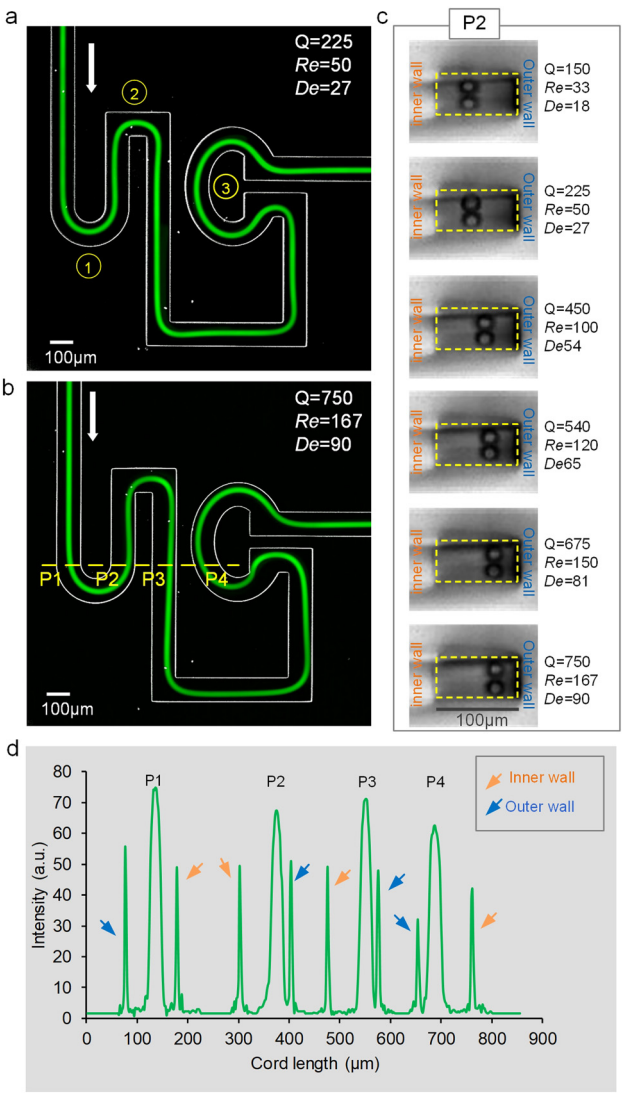

FIG. 4. Outward migration of particles in a curved channel. (a) Particle trajectories indicated by the fluorescent streak (top view) inside the microchannel at Q = 225 μl/min flow rate. (b) Top view image of the same location at Q = 750 μl/min. The P1, P2, P3, P4 downstream positions where four cross sections were imaged are indicated. Fluorescent images were stacked from 1000 frames. (c) Dynamics of the focusing positions at P2 in response to flow rate. Images were stacked from two particles. (d) Linescan of a fluorescent top view image used to determine particle lateral positions for downstream positions P1, P2, P3, and P4 as marked in panel (a). Orange and blue arrows indicate inner and outer walls for each downstream position. Particles 26.3 μm in diameter were used. Medium density was 1.055 g/ml, matching particle density. Cord length is the length of the line scan [the yellow dashed line in panel (b)].

channel. At a low flow rate (e.g., Q = 225 μl/min, $De = 27$), particles migrated toward the inner wall of the curved channel regardless of the change of curvature direction [Fig. 4(a)]. For example, particles moved upward to the inner wall at turn (1) and downward at turn (2) when the direction of curvature was flipped. It is more evident that particles moved toward the new inner wall at turn (3) when the curvature was rotated 90°. Such constant inward migration of particles agrees with observations in spiral channels where particles were found of focusing near the inner wall. At higher flow rate (e.g., Q = 750 μl/min, $De = 90$), however, particles always moved toward the outer wall despite changes in curvature orientation and different layout of the curvatures [Fig. 4(b)].

Regardless of the changes in flow rate and thus the migration direction, two positions were consistently observed in the channel cross section [Fig. 4(c)]. Early work[38] suggested that at higher flow rate particles move away from the inner wall after reaching their single equilibrium position in the vertical center plane. On the contrary, our cross-sectional images [Fig. 4(c)] reveal that particles remained in two vertical positions when they gradually migrate

laterally toward the outer wall in the U-shaped channel as the flow rate increased. Note that the starting positions of particles are the same in the cross section (P1) due to pre-focusing in the straight channel, despite different flow rates. The two vertical positions were observed throughout the channel without merging into single position, as also confirmed in Fig. 3(b)(iii) for the 18.7-μm-diameter particles. These results confirm that there are two focusing positions (or more considering the counter-rotating Dean vortices as implied by the observation of streak breakdown by Martel and Toner[39]) but only one focused stream in the top view is observed.

At low flow rate (Q = 150 μl/min, De = 18), the two positions in the cross section were closer to the inner wall at P2, the end of the U-shaped channel [Fig. 4(c)]. However, they relocated to the outer wall at De = 90 (Q = 750 μl/min), which is confirmed by line-scan of the top view image [Fig. 4(d)], where peaks of focused particles at P2, P3, and P4 are closer to the outer walls after flowing through curved segments. The distances between particle mass centers and the outer walls were 26 μm, 26 μm, and 34 μm, respectively.

In curved channels, particle migration dynamically changes in response to alterations in flow. Measurements of particle lateral position confirm that particles can move either left or right depending on the flow rate and thus on the Dean number [Eq. (1)]. However, due to the variation of curvature across P1–P4, we only investigate particle migration in the U-shaped segment (P1 and P2) in the following discussion. As shown in Fig. 5(a), due to the initial two-stage focusing in the upstream straight channel segment, particles entered the U-shaped segment at approximately the same lateral position (P1) for all the Dean numbers tested (<4 μm displacement across the De range of 12 to 119). However, the lateral position of particles at the end of the U-shaped channel (P2) increased almost linearly with De after an initial dip at De = 18. There was almost no lateral displacement of particles at De = 36 for 26.3-μm-diameter particles, where the two curves (P1 and P2) cross each other, suggesting zero net lateral force exerted on particles in the U-shaped channel. This De is termed critical Dean number (De_c) in this work.

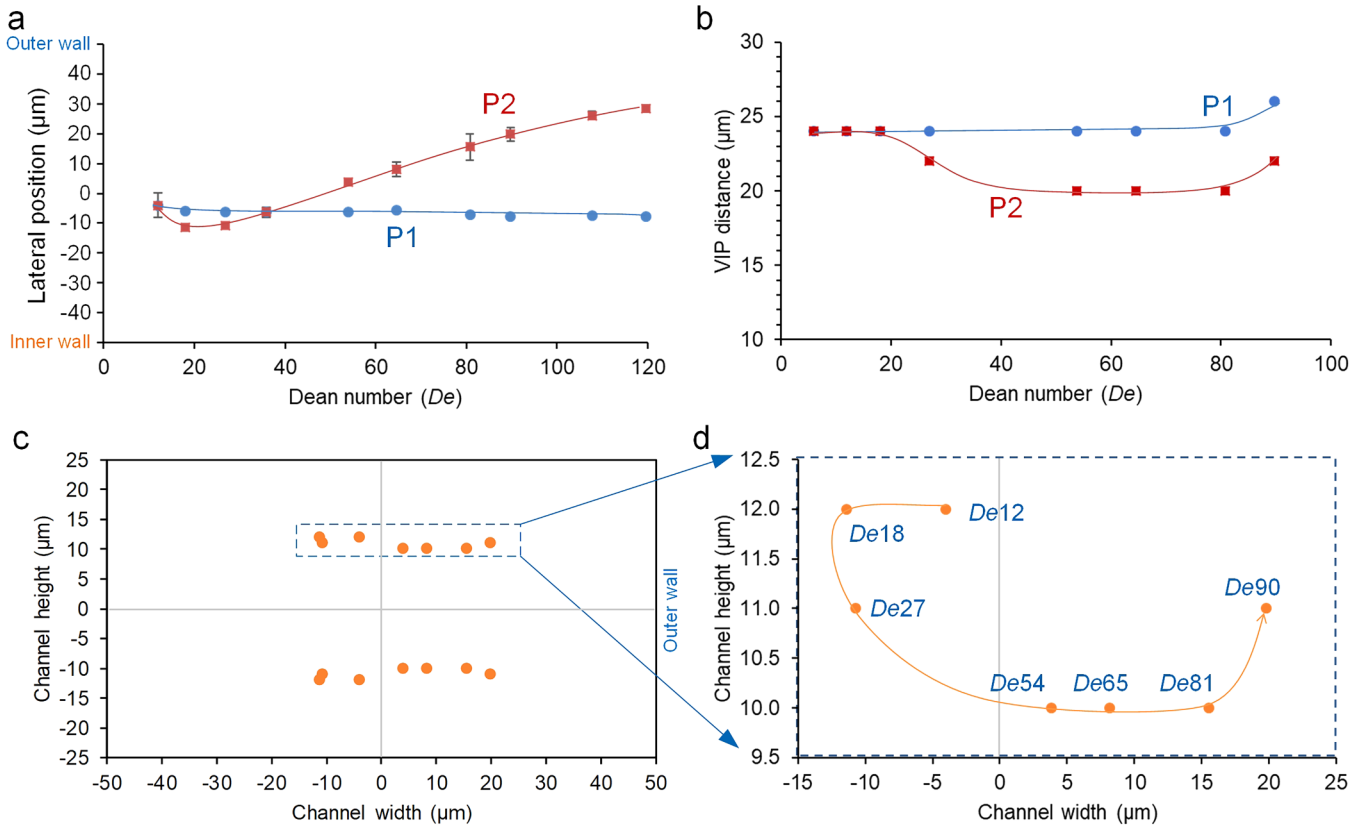

FIG. 5. Evolution of particle position in the channel cross section as Dean number increases for 26.3-μm-diameter particles. (a) Lateral position as a function of Dean number at downstream positions P1 and P2. (b) Vertical inter-position (VIP) distance as a function of Dean number at downstream positions P1 and P2. (c) Evolution of particle position in the channel cross section as Dean number increases. (d) Zoom-in of the dashed box in (c), revealing the detailed evolution path of the particle position with respect to De. Neutrally buoyant particles 26.3 μm in diameter were used. All measurements were performed in triplicate, with error bars indicating the standard deviation; in most cases the standard deviation is too small to be visible.

However, particles migrated closer to each other vertically as *De* increased [Fig. 5(b)]. The distance between the two vertical positions (mass centers of the particles) was measured to quantify the vertical movement of particles and it is termed as vertical inter-position (VIP) distance (see Fig. S3 in the supplementary material for details of this measurement). There was little change in VIP distance for $De \leq 18$, indicating no vertical movement of particles at small *De* despite the inward lateral migration [Fig. 5(a)]. As *De* increased, VIP distance is shortened. At large *De*, particles were 4 μm (8% of the 50 μm channel height) closer to each other. Even at $De = 36$ when almost no lateral displacement is observed, particles migrated toward the vertical central plane of the channel. At $De > 81$, both VIP distances at P1 and P2 increased, but the distance at P2 remained 4 μm shorter than that at P1.

Combining the lateral and vertical movements, we can attempt to resolve particle hydrodynamics in the cross section of a curved channel as a function of flow rate. In general, particles appear to cross the channel centerline and move toward the outer wall with increased flow rate [Fig. 5(c)]. The close-up panel of the dashed box [Fig. 5(d)] reveals the details of the shifting path of the particle positions in the cross section. Unfortunately, the lateral position could not be accurately determined for $De < 12$, since tight pre-focusing was not obtained in the straight upstream channel segment, and for $De > 90$, since multiple focused streams formed due to insufficient length of the pre-focusing segment. Nevertheless, the shifting path with increasing *De* is clearly visible and resembles the Dean vortices in the cross section (Fig. S3 in the supplementary material), suggesting Dean force dominates particle migration.

Although particles appeared to migrate toward the corner at $De > 81$, they were never in proximity to the outer wall and the closest position was 21 μm from the outer wall ($De = 119$). Considering the radius of the particles, a 16 μm gap remained between the nearest surface of focused particles and the channel outer wall. The particle positions seem to be related to the positions of the eyes of the two counter-rotating Dean vortices in the cross section at halfway of the U-shaped channel as indicated by the numerical models (Pm in Fig. S2 in the supplementary material). For example, particle position was measured to be (20 μm, 11 μm) from centerlines in the upper right quadrant of the channel cross section, while the eye position of the Dean vortex was at (20 μm,12 μm) for $De = 90$. This suggests that particles might be trapped in the eyes of Dean vortices at higher *De*.

Size and density dependence in curved channels

Smaller particles move faster toward the outer wall as *De* increases. To confirm this, we examined migration of the 18.7 μm-diameter ($\beta = 0.28$) and the 26.3 μm-diameter ($\beta = 0.39$) particles. Both particles shared the same initial positions at P1 due to pre-focusing in the upstream straight channel segment. Results show that the lateral position of both particle sizes increased monotonously at P2 toward the outer wall of the cross section with respect to flow rate, as indicated by the shifted curves in Fig. 6(a). For the 18.7-μm-diameter particles, the critical $De_c = 27$ when no net lateral migration was observed. Compared to the larger 26.3-μm-diameter particles with $De_c = 36$, these particles migrated faster toward the channel outer wall. When $De > 54$, the end lateral position at P2 of the smaller particles was approximately 6 μm closer to the outer wall, suggesting that separation is possible. Particles smaller than 18.7 μm in diameter were not tested since they cannot be pre-focused into the two initial positions in the cross section due to insufficient length of the straight channel segment prior to the U-shaped channel.[22] Results of even larger 32.3-μm-diameter particles ($\beta = 0.48$) show similar but downward shifted trend with $De_c \sim 46$ [Fig. 6(a)].

The existing explanation of size-dependent migration in the curved channel is not able to explain our observations that smaller particles migrate further away from the inner wall even when particles are near the outer wall. To date, the balance of Dean drag force and shear-induced lift force is considered to be responsible for the focusing of particles in spiral channels, leading to equilibration of larger particles closer to the inner wall.[23,38] However, herein particles crossed channel centerline into the region closer to the outer wall, where Dean force and lift force are in the same direction, toward the outer wall. Since both forces are strongly dependent on the particle size, the 26.3-μm-diameter particles are expected to exhibit faster lateral migration and thus should have been closer to the outer wall, which is inconsonant with our observations.

Due to the curvature of the channel, we found particle density imposed a significant effect on the outward migration of particles. We note that densities of particles and suspending solutions were not matched in early reports,[25,37,38] which serve as the basis of the current explanation. To investigate if density mismatch would change the relative lateral positions of the two particles, additional experiments were conducted using particles suspended in water (0.9982 g/ml) instead of NaCl solution (1.055 g/ml) to purposely induce a mismatch. Figure 6(b) shows lateral position as a function of Dean number for both conditions at P1 and P2 for the 18.7-μm-diameter particles. Initial positions were nearly the same at P1 for the two conditions, indicating little impact of density on the inertial focusing in the straight channel. At small *De*, particles shared similar outward migration velocity. However, as the *De* increased, particles in water migrated slightly faster and were closer (e.g., 6 μm closer at $De = 81$) to the outer wall than those neutrally buoyant particles in the NaCl solution.

Similar effect of density mismatch for the 26.3-μm-diameter particles is shown in Fig. S4 in the supplementary material, however, the 18.7-μm-diameter particles were still closer to the outer wall (e.g., 5 μm closer at $De = 81$). Such differentiated migration is reasonable, considering the strong centrifugal force acting on particles at higher flow rates. Comparison of the calculated Dean force and centrifugal force can be found in Fig. S5 in the supplementary material. Nevertheless, the addition of centrifugal force does not explain the relative positions of the 18.7 and 26.3-μm-diameter particles as larger particles would experience stronger centrifugal force which is in the same direction of Dean force.

Considering the migration dynamics in the cross section offers an opportunity to reconcile discrepancies between our observations and the existing explanation. Measurements of VIP distance for the 18.7-μm-diameter particles show that they first migrate vertically closer to each other (thus toward the vertical center plane) as *De* increased [Fig. 6(c)]. Even in the absence of lateral migration

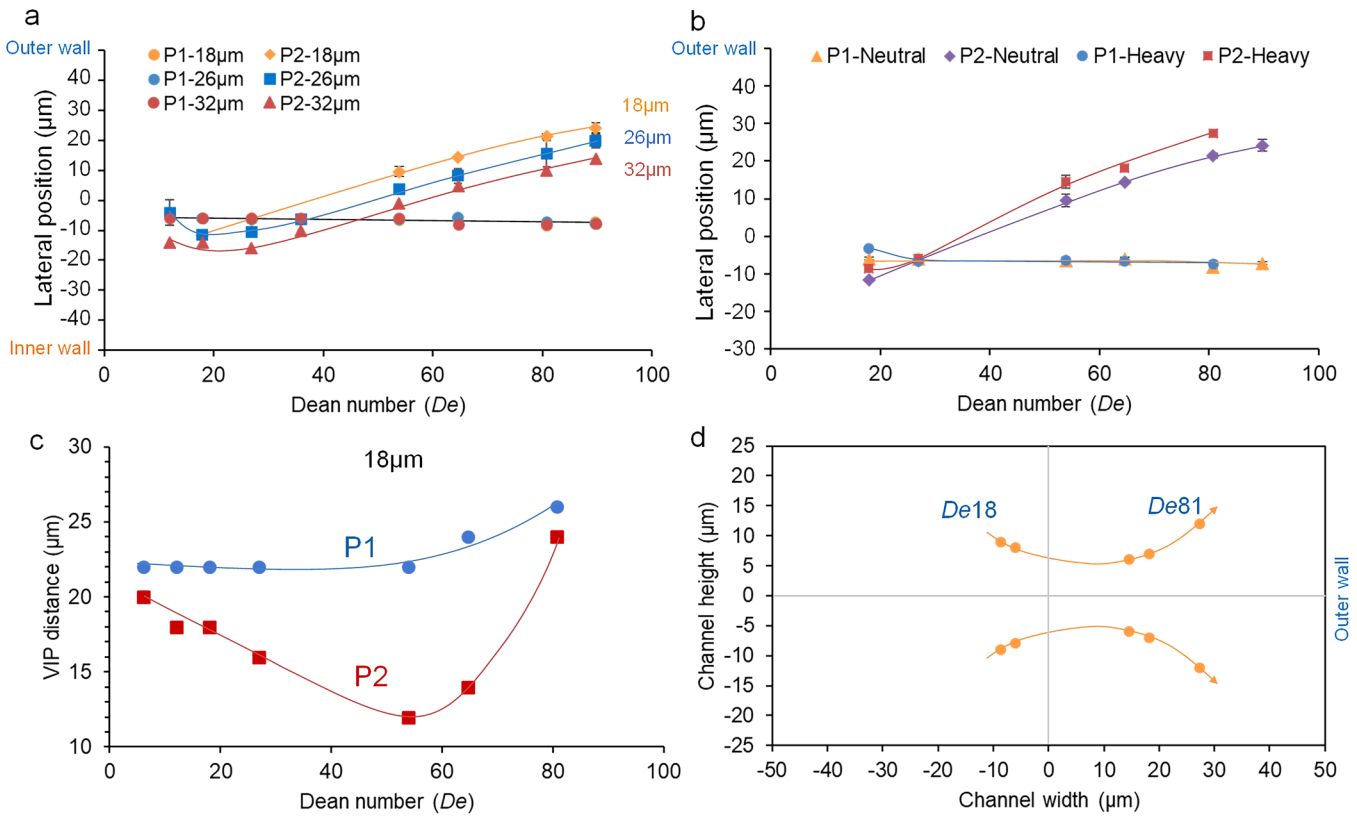

FIG. 6. Effect of particle size and density mismatch on migration. (a) Lateral position as a function of Dean number for the 18.7-μm-, 26.3-μm-, and 32.3 μm-diameter particles at downstream positions P1 and P2. Densities of particle and medium were matched by adding NaCl to DI water. (b) Lateral position as a function of Dean number for 18.7-μm-diameter particles suspended in low-density medium (DI water ~0.9982 g/ml, heavy particles) and matched density medium (1.055 g/ml, neutrally buoyant particles) at downstream positions P1 and P2. (c) Vertical inter-position (VIP) distance as a function of Dean number for 18.7-μm-diameter particles. (d) Evolution of 18.7-μm-diameter particle position in the cross section at P2 as *De* increases. Data points with $De < 10$ cannot be plotted here as particles were not laterally focused. Since two weak side streams formed when $De > 54$, only the lateral position of the major central particle stream was measured and presented in this figure.

at $De = 27$, particles are 8 μm (16% of channel height) closer to each other at the end (P2) as compared to the beginning (P1) of the U-shaped channel. At $De > 54$, particles vertically migrate toward the bottom and top channel walls as the VIP distance increases. Nonetheless, the 18.7-μm-diameter particles are always closer to the channel center plane than the 26.3-μm-diameter particles when $De < 81$ [Figs. 5(c) and 5(d) and 6(c)and 6(d)]. Note that Dean velocity is maximized in the center plane (Fig. S3 in the supplementary material) and thus the smaller particles experience stronger Dean force which is proportional with Dean velocity.[38] The stronger Dean force and thus faster Dean velocity drive smaller particles faster and closer to the outer wall. On the other hand, since the 26.3-μm-diameter particles are closer to the top or bottom walls, they are subjected to two opposing Dean forces laterally: (1) a Dean force in the direction of the inner wall and acting on one side of the particle closest to the top or bottom wall, and (2) a Dean force directing to the outer wall acting on the other side of the particle closest to the channel center plane. As a result, the net Dean force acting on larger particles is smaller than that of the smaller particles. Thus, the difference in the vertical position leads to the faster outward migration of smaller particles despite Dean force scaling with particle size.

The determinant role of particle vertical position suggests both inward and outward migration can exist concurrently. Figure 7 shows the downstream trajectories of three individual 18.7-μm-diameter particles located at different initial lateral positions. The particle initially near the outer wall migrated inward as it traveled through the U-shaped channel [Fig. 7(a)], while the particles initially at the center or closer to the inner wall migrated outward [Figs. 7(b) and 7(c)]. The migration velocity of the outer wall particle was −163 mm/s, while the inner wall particle migrated at 400 mm/s and the center particle migrated at 175 mm/s. The migration trends of these particles followed the streamlines in general [Fig. 7(d)]. Particle positions in the cross section [Fig. 7(d) inset] reveal that the particles initially near the outer wall are closest to the top or bottom wall, while the particles initially at the center or near the inner wall are closer to the vertical center plane. These results confirm that the differential migration dynamics depends on the particle vertical position.

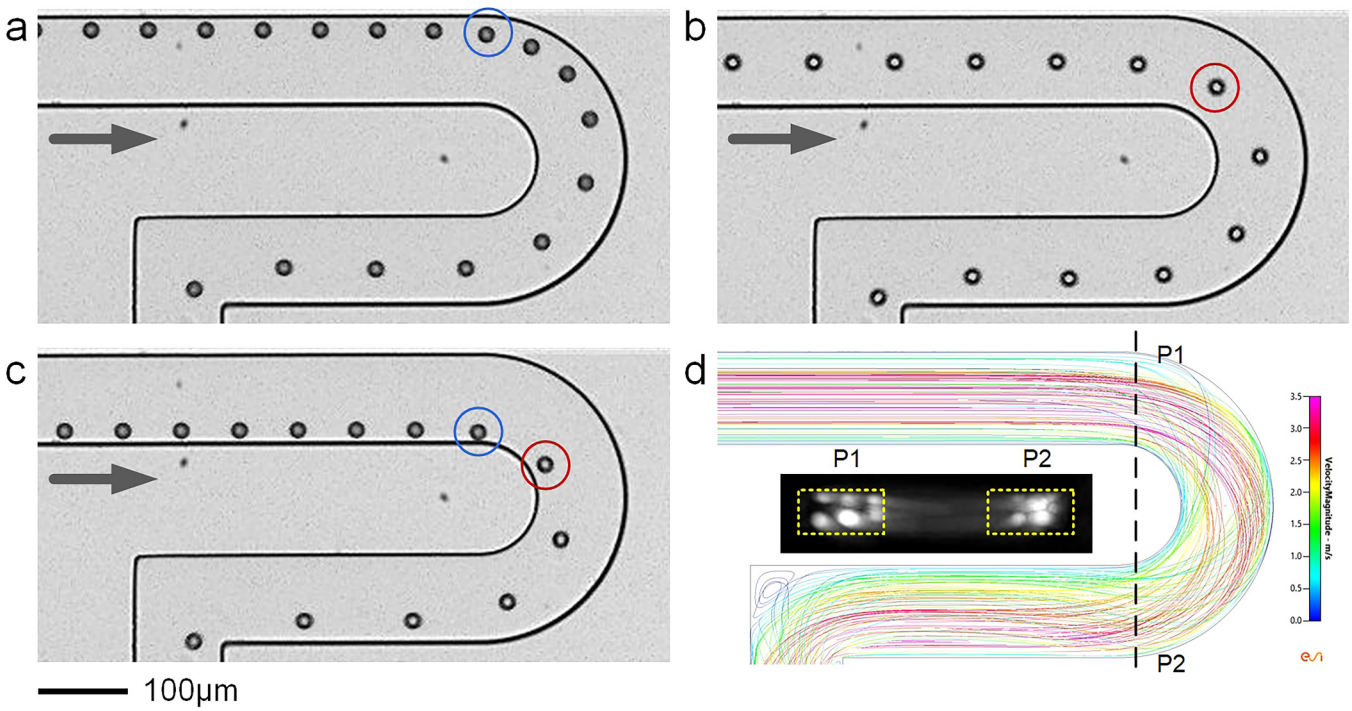

FIG. 7. Migration dynamics depends on the initial position of particles in the channel cross section. Stacked images of the high-speed camera (25 000 fps) show downstream migration of three individual particles initially located near (a) outer wall, (b) center, and (c) inner wall (c). Particle in (b) is at different vertical plane as indicated by the differences of shading (bright vs dark spheres). Particle in (c) changes vertical position as it moves downstream. (d) Streamlines from simulation and particle positions in the cross section (inset stacked fluorescent image) for P1 and P2, which indicate all the three particles in (a–c) were not in the same vertical plane. Particle in (a) was closer to the channel top or bottom wall, the one in (c) was initially closer to the center plane, and the one in (b) was in between. Flow rate was 540 μl/min ($De = 65$) and particles were 18.7 μm in diameter.

DISCUSSION

We have demonstrated a direct method of imaging through the cross section of a microchannel, which provides critical information on the dynamics of particle inertial migration in both straight and curved microchannels. In a rectangular straight microchannel, particles stay unfocused at low Reynolds number and are focused into two layers near long edges of the channel cross section as Reynolds number increases and inertial forces become dominant. These two layers of particles further condense into two positions at the centers of the long edges of the cross section when Reynolds number exceeds a critical value for a channel with given downstream length. These new results from the cross-section view offer a confirmation of our two-stage model of inertial migration inferred from the top view and side view images.[22]

In curved microchannels, a dynamic picture of 3D inertial migration of particles has been achieved using the combination of top view and cross-section images. Our new findings reveal that particles migrate toward the inner wall at $De < De_c$ and toward the outer wall at $De > De_c$ (Fig. 8). The net lateral force acting on particles should be zero at $De = De_c$, since no lateral displacement of particles from P1 to P2 was found. This critical De appears to be size-dependent (e.g., $De_c \sim 27$ for 18.7 μm particles, $De_c \sim 36$ for 26.3 μm particles, and $De_c \sim 46$ for 32.3 μm particles). In a spiral channel with the same cross section, Martel and Toner[24] suggested the ratio of $\beta/\sqrt{D_h/(2R)}$ as the criterion for the inward or outward migration. If $\beta/\sqrt{D_h/(2R)} > 2$, then the migration should be toward the inner wall; otherwise, the migration should be toward the outer wall. In our case, such ratios for both particles are less than 1, and particles should migrate outward, which seems in good agreement largely with the prediction. However, our results also show that both particles migrated toward the inner wall at $De < De_c$ even when $\beta/\sqrt{D_h/(2R)} < 2$, suggesting the criterion should be revised to include flow condition.

We found that there exists a critical dimensionless ratio ($\beta/De_c \sim 0.01$) that determines particle migration direction in curved channels, such as single-loop channels with constant radius of curvature or spiral channels with varying radius of curvature. Particles migrate outward when $\beta/De < 0.01$ and inward when $\beta/De > 0.01$. This criterion holds true for all the three particle sizes in this work (32.3 μm, 26.3 μm, and 18.7 μm) as shown in Fig. 9(a). To examine the applicability of our findings to other particle sizes and channel geometries, we analyzed data reported in previous studies by us and others,[23,24,38,40] where the change of migration direction of focused particles was experimentally documented. The results are shown together with our data in Fig. 9(b), where a total of 32 data points generated from 10 particle sizes (4.4–32.3 μm) and 12

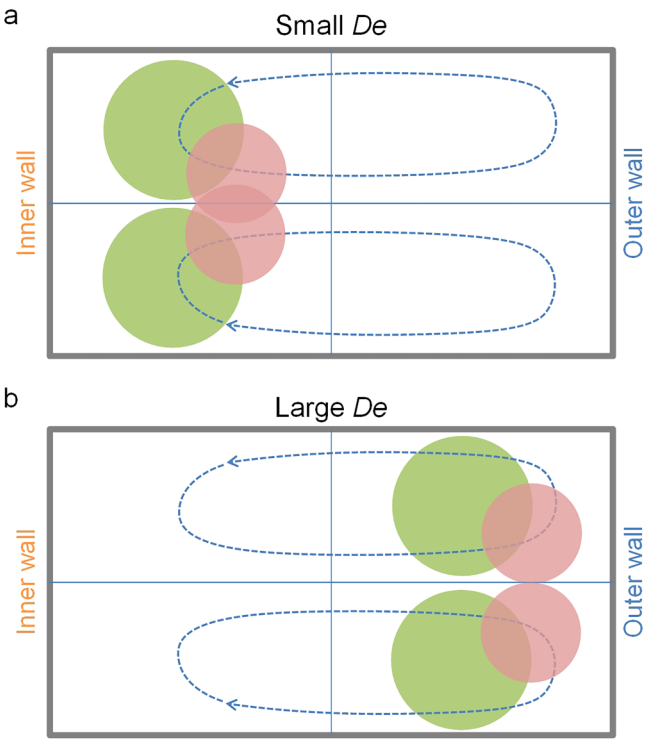

FIG. 8. Graphic illustration of size-dependent particle focusing in the cross section of a low AR curved channel. (a) At small *De*, particles focus near the inner wall with smaller particles vertically closer to the center plane but horizontally further away from the inner wall. (b) At large *De*, particles focus in the outer half of the cross section, with smaller particles vertically closer to the center plane and horizontally closer to the outer wall.

geometries with various aspect ratios (0.13–0.50) are present. The blockage ratio ranges from 0.045 to 0.48 for these data. Due to the constant change of Dean number in spiral channels, we used the average Dean number (average of *De* at the beginning and end of the spiral channel) in determining the De_c. As shown by the linear regression, $\beta/De_c \sim 0.01$ with $R^2 > 0.98$. Outward migration occurred for data below the fitted line and inward migration recorded for those above the line. As a result, our finding of the dimensionless ratio β/De is applicable in predicting particle migration direction over a wide range of particle sizes and channel geometries, including the most common spiral channels.

The identified dimensionless number ($\beta/De \sim 0.01$) can be a practical design guideline for the development of curved separation systems. This ratio $\left(\frac{\beta}{De} = \frac{a}{Re}\sqrt{\frac{2R}{D_h^3}}\right)$ relates particle size, channel geometry, and flow condition to the inertial migration dynamics. In the premise of particles reaching focusing ($Re_p > 1$),[1] our expression of $\beta/De \sim 0.01$ indicates that larger particles need larger *De* for outward migration and smaller particles can migrate outward at smaller *De*. This suggests there is an intermediate range of *De* where particles can undergo opposing migration directions (e.g., inward and outward for larger and smaller particles, respectively), leading to particle separation in a curved channel. Such implication is consistent with the existing reports on particle separation in spiral channels.[37,38,41–43] On the other hand, this expression also suggests that small *De* (larger radius of curvature) is preferred for inward migration of particles and that larger cross section (D_h) is preferred for inward migration at higher throughput, which is the case of most spiral separation systems (several hundreds of microns of channel width and ml/min throughput).[38,41–43] Our expression estimates the critical Dean number (De_c) for a given channel and a given particle size. The De_c is underestimated when the inner most radius of curvature is used for a spiral channel with deceasing *De* downstream the channel. Nevertheless, the general trend of increasing De_c for larger particle was evidenced in other work of spiral channels.[38,40]

Our results of mapping the shifting path of particle positions in the cross section indicate that inertial migration of particles in curved channels is in 3D as they travel downstream [Figs. 5(d) and 6(d)]. Particles migrate not only laterally but also vertically in the cross section (Fig. 8). Even when there is no net lateral migration at $De = De_c$, particles migrate vertically in the cross section [Figs. 5(d) and 6(d)] Such observation was also implied by Martel and Toner[24] despite the absence of clear evidence. When particles stay in proximity to channel walls, they migrate inward; conversely, they migrate outward and move vertically closer to the channel center plane where Dean velocity and thus Dean force are maximized. The shifting path seems related to the Dean vortices in general, as also suggested in the early work by Gossett and Di Carlo.[25]

Nevertheless, the merging of two vertical positions into a single focusing position in the center plane was not observed in this work. This is reasonable considering the shear-induced lift force driving particles toward the top and bottom walls in a low aspect ratio (AR) rectangular channel (Fig. 8). On the other hand, the direction of shear-induced lift force may change in the curved channel due to the redistribution of velocity profile[44] (Fig. S6 in the supplementary material), leading to the possibility of single focusing position near the inner wall. In a high AR channel, the two vertical positions may come close enough and maybe appear as single position, as the shear-induced lift force changes direction and aligns with Dean force. Further experimental validation is required. In terms of the number of vertical positions, it can be two or more [see Fig. 7(d) inset] considering the recirculation of the two Dean vortices, each of which can have one or two positions (one shall be metastable if two).

Smaller particles come closer to the vertical center plane, leading to faster outward migration due to faster Dean velocity. The 18.7-μm-diameter particles appeared to migrate steadily to the vertical center plane [Fig. 6(d)] as they migrated outward when $De < 65$. Such migration toward the center plane might be due to the Dean vortices or due to that the presence of Dean vortices disrupted the velocity profile near channel walls and thus changes the otherwise strong shear-induced lift force which confines particles to sidewalls in straight channels.[22] The outward migration velocity of these smaller particles was unexpectedly faster than the larger 26.3-μm-diameter particles. Considering the scaling of the Dean force with the particle diameter, the larger particles migrate faster.[37,38] Such discrepancy is reconciled by the fact that these two

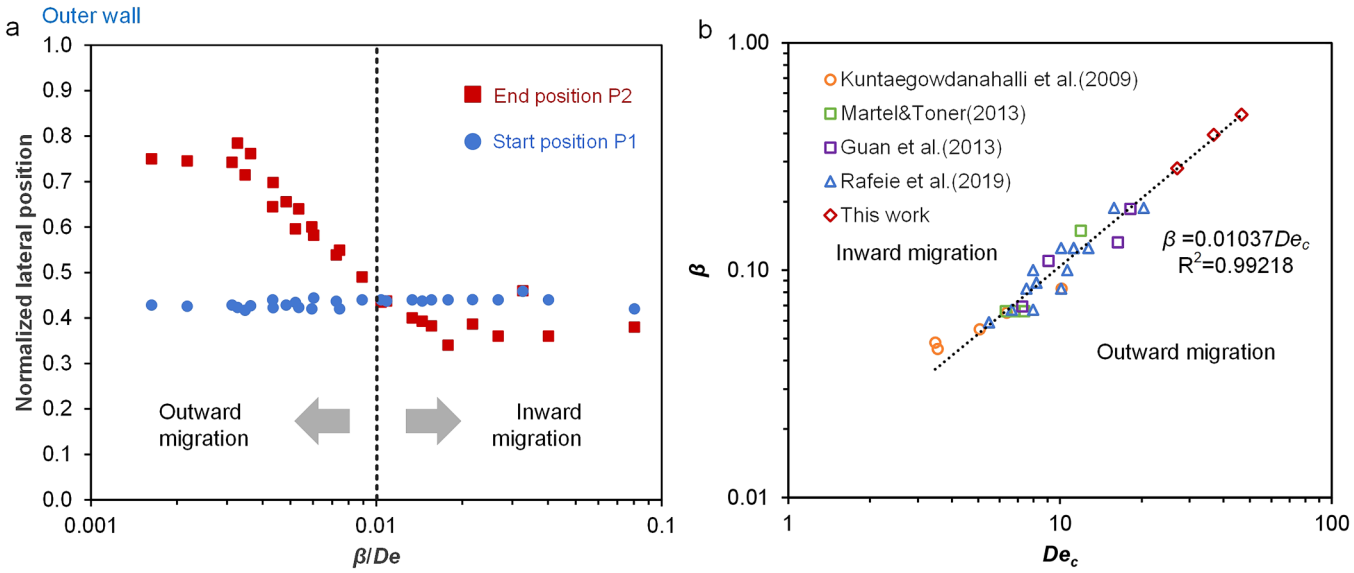

FIG. 9. The ratio β/De determines migration direction in curved channels. (a) State diagram showing particle migration direction determined by β/De. Data points represent measurements of three particle sizes (18.7, 26.3, and 32.2 μm) at various flow rates. (b) Aggregated data from this work and other investigators, illustrating that the ratio of $\beta/De_c \sim 0.01$ is broadly applicable to other particle sizes in spiral channels. Data from curved and spiral channels with rectangular cross sections in works by Kuntaegowdanahalli *et al.*,[38] Martel and Toner,[24] Guan *et al.*,[23] and Rafeie *et al.*[40] were analyzed to identify the critical Dean numbers (De_c) for smaller blockage ratios (β). Due to the constantly changing De in spiral channels, an average Dean number was used in determining the critical Dean number De_c.

particles were vertically located in different positions [Figs. 5(d) and 6(d)], with the smaller particles closer to the center plane. Besides, larger particles might experience two opposing Dean forces due to their large size spanning both directions of the Dean vortex. In this regard, tuning particle vertical positions can enhance the separation performance in curved channels. This practically can be done by adjusting Dean number [Fig. 6(a)] or by designing a multi-inlet system that introduces particles into specific regions of the channel cross section (e.g., regions near the top and bottom walls in the inner half of the cross section). Additionally, we found that slight mismatch of particle and fluid densities did not affect particle focusing in the straight channel, but it became significant in the curved channel at large Dean number.

Centrifugal force due to slight particle-density mismatch becomes significant when $De > De_c$. Lateral displacements of particles due to this additional centrifugal force were evident for both 18.7 μm and 26.3-μm-diameter particles [Fig. 6(b) and Fig. S4 in the supplementary material]. As much as 6 μm difference in lateral displacement was observed for both particles due to the density mismatch at $De = 81$. Such difference decreases at even higher De, suggesting there should be a stronger counteracting force at larger De. This counteracting force can be wall-induced lift force when particles are closer to the outer wall. However, the closest distance between the particle surface and outer channel wall for 26.3 μm particles was 13 μm, which may be still quite far away to significantly increase wall-induced lift force. Another possibility is that particles are subjected to stronger Dean force directing to the inner wall at larger De. As we discussed, particles are subjected to two opposing lateral Dean forces due to their physical size. Inward Dean force may become stronger as particles are closer to the top and bottom walls at larger De [Figs. 5(d) and 6(d)], leading to smaller net Dean force directing outward. Additionally, due to the redistribution of velocity profile in the curved channel (Fig. S6 in the supplementary material), it is possible that there is a shear-induced lift force directing at the inner wall and counteracting the centrifugal force. These findings suggest practically density mismatch should be considered when designing a curved channel for separation at high throughput and separation based on density is possible in curved channels.

We note that there are some limitations in our work. First, we used large particle blockage ratios ($\beta \geq 0.28$) to achieve pre-focusing of particles in the straight upstream segment prior to the U-shaped channel. This was to ensure particles start at the same cross-sectional position upon entering the curved channel. As a result, migration dynamics of particles of smaller blockage ratio was not tested. However, analysis of results by other investigators[23,24,38,40] indicates that our finding of the dimensionless number ($\beta/De \sim 0.01$) is applicable to a wide range of blockage ratios (0.045–0.48) [Fig. 9(b)]. Second, only results of low AR rectangular channels were discussed. We tested one channel geometry in this work and analyzed 11 geometries from other investigators,[23,24,38,40] but all of the channel cross sections were low AR rectangles [AR ranging from 0.13 to 0.5 in Fig. 9(b)]. In high AR channels, due to the direction change of shear-induced lift force, the migration dynamics in the cross section might be different. Early work by Gossett and Di Carlo[25] suggested a possible single focusing position in a high AR U-shaped channel, but this is yet to be reported

in the literature. Third, the Dean vortices at the end of the U-shaped segment may be weaker than those in the middle of the segment (Fig. S2 in the supplementary material) due to the influence of the following straight segment. This change of vortex strength may slightly affect our critical Dean number. Additional future work is necessary to address these limitations and to further elucidate inertial dynamics in curved channels.

SUPPLEMENTARY MATERIAL

See the supplementary material for the illustration of surface smoothing of the cutting surface for device imaging, numerical modeling of Dean vortices in the channel cross section, vertical displacement of the 18.7-μm- and 26.3-μm-diameter particles as a function of flow rate, and comparison of the Dean force and the centrifugal force for 18.7-μm-diameter particles.

ACKNOWLEDGMENTS

We gratefully acknowledge partial support from the NSF Center for Advanced Design and Manufacturing of Integrated Microfluidics (CADMIM), NSF Award No. IIP-1841473, and from the Richard and Loan Hill Department of Bioengineering at the University of Illinois at Chicago.

DATA AVAILABILITY

The data that support the findings of this study are available from the corresponding author upon reasonable request.

REFERENCES

[1]J. Zhou, P. Mukherjee, H. Gao, Q. Luan, and I. Papautsky, APL Bioeng. **3**, 041504 (2019).
[2]J. Zhang, S. Yan, D. Yuan, G. Alici, N.- Nguyen, M. Ebrahimi Warkiani, and W. Li, Lab Chip **16**, 10–34 (2016).
[3]Z. Wu, Y. Chen, M. Wang, and A. J. Chung, Lab Chip **16**, 532–542 (2016).
[4]H. W. Hou, R. P. Bhattacharyya, D. T. Hung, and J. Han, Lab Chip **15**, 2297–2307 (2015).
[5]J. Zhou, A. Kulasinghe, A. Bogseth, K. O'Byrne, C. Punyadeera, and I. Papautsky, Microsyst. Nanoeng. **5**, 8 (2019).
[6]A. Kulasinghe, J. Zhou, L. Kenny, I. Papautsky, and C. Punyadeera, Cancers **11**, 89 (2019).
[7]H. Haddadi, H. Naghsh-Nilchi, and D. Di Carlo, Biomicrofluidics **12**, 014112 (2018).
[8]E. Ozkumur, A. M. Shah, J. C. Ciciliano, B. L. Emmink, D. T. Miyamoto, E. Brachtel, M. Yu, P.- Chen, B. Morgan, J. Trautwein, A. Kimura, S. Sengupta, S. L. Stott, N. M. Karabacak, T. A. Barber, J. R. Walsh, K. Smith, P. S. Spuhler, J. P. Sullivan, R. J. Lee, D. T. Ting, X. Luo, A. T. Shaw, A. Bardia, L. V. Sequist, D. N. Louis, S. Maheswaran, R. Kapur, D. A. Haber, and M. Toner, Sci. Transl. Med. **5**, 1–11 (2013).
[9]N. Godino, F. Jorde, D. Lawlor, M. Jaeger, and C. Duschl, J. Micromech. Microeng. **25**, 084002 (2015).
[10]M. S. Syed, M. Rafeie, D. Vandamme, M. Asadnia, R. Henderson, R. A. Taylor, and M. E. Warkiani, Bioresour. Technol. **252**, 91–99 (2018).
[11]B. R. Mutlu, J. F. Edd, and M. Toner, Proc. Natl. Acad. Sci. U.S.A. **115**, 7682–7687 (2018).
[12]J. Cruz, T. Graells, M. Walldén, and K. Hjort, Lab Chip **19**, 1257–1266 (2019).
[13]C. Tesauro, B. Ferrando, X. Ma, M. Jepsen, A. Ivarsen, R. Frøhlich, T. Stevnsner, B. Knudsen, and Y. Ho, RSC Adv. **7**, 23735–23741 (2017).
[14]D. R. Gossett, H. T. K. Tse, J. S. Dudani, K. Goda, T. A. Woods, S. W. Graves, and D. Di Carlo, Small **8**, 2757–2764 (2012).
[15]A. J. Mach, J. H. Kim, A. Arshi, S. C. Hur, and D. Di Carlo, Lab Chip **11**, 2827–2834 (2011).
[16]C. Tu, J. Zhou, Y. Liang, B. Huang, Y. Fang, X. Liang, and X. Ye, Biomed. Microdevices **19**, 83 (2017).
[17]J. M. Martel, K. C. Smith, M. Dlamini, K. Pletcher, J. Yang, M. Karabacak, D. A. Haber, R. Kapur, and M. Toner, Sci. Rep. **5**, 11300 (2015).
[18]Y. Deng, M. Kizer, M. Rada, J. Sage, X. Wang, D. Cheon, and A. J. Chung, Nano Lett. **18**, 2705–2710 (2018).
[19]D. R. Gossett, H. T. Tse, S. A. Lee, Y. Ying, A. G. Lindgren, O. O. Yang, J. Rao, A. T. Clark, and D. Di Carlo, Proc. Natl. Acad. Sci. U.S.A. **109**, 7630–7635 (2012).
[20]J. M. Martel and M. Toner, Annu. Rev. Biomed. Eng. **16**, 371–396 (2014).
[21]H. Amini, W. Lee, and D. Di Carlo, Lab Chip **14**, 2739–2761 (2014).
[22]J. Zhou and I. Papautsky, Lab Chip **13**, 1121–1132 (2013).
[23]G. Guan, L. Wu, A. A. Bhagat, Z. Li, P. C. Chen, S. Chao, C. J. Ong, and J. Han, Sci. Rep. **3**, 1475 (2013).
[24]J. M. Martel and M. Toner, Sci. Rep. **3**, 3340 (2013).
[25]D. R. Gossett and D. Di Carlo, Anal. Chem. **81**, 8459 (2009).
[26]S. C. Hur, A. J. Mach, and D. Di Carlo, Biomicrofluidics **5**, 022206 (2011).
[27]J. Kim, J. Lee, C. Wu, S. Nam, D. Di Carlo, and W. Lee, Lab Chip **16**, 992–1001 (2016).
[28]P. Mukherjee, X. Wang, J. Zhou, and I. Papautsky, Lab Chip **19**, 147–157 (2019).
[29]H. Feng, J. J. Magda, and B. K. Gale, Appl. Phys. Lett. **115**, 263702 (2019).
[30]Y. S. Choi and S. J. Lee, Microfluid. Nanofluid. **9**, 819–829 (2010).
[31]K. W. Seo, Y. S. Choi, and S. J. Lee, Exp. Fluids **53**, 1867–1877 (2012).
[32]T. D. Nguyen, V. T. Tran, Y. Q. Fu, and H. Du, Appl. Phys. Lett. **112**, 213507 (2018).
[33]H. Shichi, H. Yamashita, J. Seki, T. Itano, and M. Sugihara-Seki, Phys. Rev. Fluids **2**, 044201 (2017).
[34]P. Mukherjee, F. Nebuloni, H. Gao, J. Zhou, and I. Papautsky, Micromachines **10**, 192 (2019).
[35]J. Zhou, P. V. Giridhar, S. Kasper, and I. Papautsky, Biomicrofluidics **8**, 044112 (2014).
[36]D. Di Carlo, D. Irimia, R. G. Tompkins, and M. Toner, Proc. Natl. Acad. Sci. U.S.A. **104**, 18892–18897 (2007).
[37]A. A. S. Bhagat, S. S. Kuntaegowdanahalli, and I. Papautsky, Lab Chip **8**, 1906–1914 (2008).
[38]S. S. Kuntaegowdanahalli, A. A. S. Bhagat, G. Kumar, and I. Papautsky, Lab Chip **9**, 2973–2980 (2009).
[39]J. M. Martel and M. Toner, Phys. Fluids **24**, 032001 (2012).
[40]M. Rafeie, S. Hosseinzadeh, R. A. Taylor, and M. E. Warkiani, Biomicrofluidics **13**, 034117 (2019).
[41]L. Wu, G. Guan, H. W. Hou, A. A. S. Bhagat, and J. Han, Anal. Chem. **84**, 9324–9331 (2012).
[42]N. Nivedita and I. Papautsky, Biomicrofluidics **7**, 054101 (2013).
[43]M. E. Warkiani, B. L. Khoo, L. Wu, A. K. P. Tay, A. A. S. Bhagat, J. Han, and C. T. Lim, Nat. Protoc. **11**, 134–148 (2016).
[44]H. De Vriend, J. Fluid Mech. **107**, 423–439 (1981).
[45]J. Zhou, Z. Peng, and I. Papautsky, Microsyst. Nanoeng. **6**, 105 (2020).